

Computer Simulations of X-Ray Spherical Wave Laue Diffraction in a Thick Perfect Crystal with a Triangular Cutout on the Exit Surface

Victor Germanovich Kohn* and Irina A. Smirnova

The results of computer simulations of X-ray spherical wave dynamical Laue diffraction in a perfect crystal of a special shape are presented. Namely, the crystal has a triangular cutout on the exit surface with the angle 2θ less than $2\theta_B$, where θ_B is the Bragg angle. The effect of a strong increase in the intensity near the triangular cutout is found in the case of a thick crystal. It is demonstrated that the X-ray beam intensity can be increased up to seven times under the conditions of the Borrmann effect. The fast Fourier transform (FFT) algorithm is used at the first step where simulations of spherical wave Laue diffraction in a perfect crystal slab are performed. Thus, the X-ray fields are obtained in front of the triangular cutout which are used as boundary conditions for the second step. At the second step, a direct numerical solution of the Takagi equations is used. The effect of a strong increase in intensity is observed for all source-to-crystal distances including the distance of diffraction focusing. This effect is explained in terms of a crystal propagator.

1. Introduction

X-ray topography is a tool for imaging inhomogeneous coherent intensity distribution due to the diffraction of X-rays in a crystal lattice. In the Laue case, this technique begins from the work by Kato and Lang,^[1] where an X-ray beam from a laboratory source was restricted by a narrow slit. Soon Kato^[2] developed the theory of X-ray spherical wave diffraction, and Takagi^[3] proposed a set of two differential equations that allows one to calculate inhomogeneous wave-field amplitudes inside a crystal in the general case.

Later on, a solution of the Takagi equations in the case of a perfect single crystal and an inhomogeneous incident wave or an uneven surface profile was derived as a convolution of the incident wave and the crystal propagator in a series of works.^[4–10] The crystal propagator has an analytical form through the Bessel functions. In the case of crystal lattice distortion, an

effective numerical method for a solution of the Takagi equations was proposed (see, for example, previous study^[11]).

The theory of X-ray spherical wave diffraction was developed further in the work by Afanas'ev and Kohn,^[12,13] where the effect of diffraction focusing was discovered under the conditions of a large source-to-detector distance. Numerous works were performed with the aim of imaging crystal lattice defects such as dislocations, stacking faults, and so on, both experimentally and theoretically (see references in the book^[14]).

In several works, the structure of inhomogeneous wave fields in a perfect single crystal of special shape was investigated. In this case, both analytical and numerical approaches can be used. Crystals with a cross-section in the scattering plane

such as a parallelepiped or a cylinder were considered in the studies.^[15–20] Recently such problems have been investigated again.^[21,22]

In this work, we investigate theoretically a problem of X-ray spherical wave diffraction in a thick perfect single crystal having the shape of a slab with a triangular cutout on the exit surface. The method of computer simulations is used. Note that such a shape of a crystal was preliminarily investigated in the early work by Afanas'ev and Kohn^[23] by means of analytical approach for a plane incident wave. The motivation for that work was an etch-pit visibility problem seen on the X-ray topographs. The effect of interference with a strong increase in the intensity was discovered. In this work, we analyze this effect in more detail and in the general case of an incident spherical wave. Our results can stimulate the experimental studies of a strong X-ray interference effect.

In the next section, the formulation of a problem and the method of computer simulations are presented. The results and discussion are presented in the subsequent sections.

2. Problem Formulation and Computer Simulation Method

We consider an experimental setup shown in **Figure 1**. The X-ray monochromatic spherical wave from the point source located at the distance L from the crystal has a finite angular divergence. The crystal shape is a slab of the thickness t with a cutout of

Dr. V. G. Kohn
National Research Centre "Kurchatov Institute"
123182 Moscow, Russia
E-mail: kohnvict@yandex.ru

Dr. I. A. Smirnova
Institute of Solid State Physics
RAS
142432 Chernogolovka, Moscow District, Russia

 The ORCID identification number(s) for the author(s) of this article can be found under <https://doi.org/10.1002/pssb.201900441>.

DOI: 10.1002/pssb.201900441

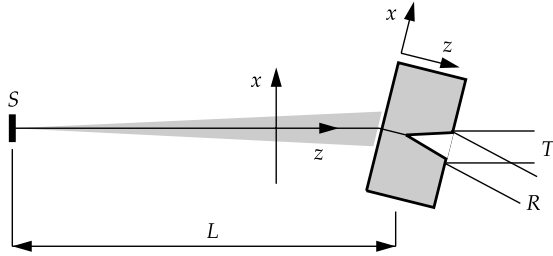


Figure 1. Experimental setup on which computer simulations are based. Here *S* is the X-ray source, *T* is the transmitted beam, and *R* is the reflected beam.

the triangular form of the height t_0 on the exit surface. In a synchrotron radiation case, each point of the transverse section of a real source can be considered as being independent of other points due to a spontaneous origin of radiation impulses (wave trains) created by separate electrons inside the bunch. Therefore, a point source only creates coherent radiation. The radiation is monochromated by a standard Si double-crystal monochromator (not shown).

The triangular cutout is a reason of spatial inhomogeneity of beam intensity measured by two detectors for both the transmitted and reflected beams. They are located at some distance from the crystal for eliminating beam interference. For the sake of simplicity, we will consider the intensity of these beams on the exit surface of the crystal. The task can be divided into two steps.

At the first step, we consider diffraction of an X-ray monochromatic spherical wave in the crystal slab of the thickness $t_1 = t - t_0$. In this case, the intensity inhomogeneity along the crystal surface (the x axis) arises from the incident spherical wave only. It is convenient to solve the task by means of Fourier transformation. At this point, the z and x coordinates are counted along and normal to the direction from the source to the crystal. The x projection of the incident wave can be described within paraxial approximation as the modified Fresnel propagator introduced by Kohn.^[24]

$$P(x, L) = (i\lambda L)^{-1/2} \exp\left(i\pi \frac{x^2}{\lambda L} - e_1 \frac{x^2}{x_r^2}\right) \quad (1)$$

where λ is the radiation wave length, $e_1 = \ln 2/2$, $2x_r = L\alpha_d$ is the beam intensity FWHM (full width at half maximum) at the distance L , and α_d is the beam angular divergence. The Fourier image of this function is equal to

$$P_r(q, L) = C_r^{-1/2} \exp\left(-i \frac{\lambda L}{4\pi C_r} q^2\right) \quad (2)$$

where $C_r = 1 + i\sigma$, $\sigma = \lambda L e_1 / \pi x_r^2$.

We consider the normalized incident wave as

$$E_i(x) = (\lambda L)^{1/2} \exp(iKz) P(x, L), \quad (3)$$

where $K = 2\pi/\lambda$. The incident wave can be represented as a superposition of plane waves by means of the Fourier integral

$$E_i(x) = (\lambda L)^{1/2} \int \frac{dq}{2\pi} \exp(iKz + iqx) P_r(q, L). \quad (4)$$

We note that $|q| \ll K$. Therefore, $q = K\theta$ describes a small angular divergence of the incident wave. The integrand is a plane wave with the wave vector $\mathbf{k}_0 = (q, 0, K)$. We assume that the crystal is oriented near the Bragg angle for symmetrical Laue diffraction with the reciprocal lattice vector \mathbf{h} . It is well known that the transmitted wave direction (the wave vector) stays unchanged due to plane wave diffraction in the crystal slab having a perfect crystal lattice.^[14,25]

Therefore, we can write the following equation for the transmitted wave

$$E_0(x, t_1) = (\lambda L)^{1/2} \int \frac{dq}{2\pi} \exp(iqx) P_r(q, L) A_0(q, t_1) \quad (5)$$

Here and below we omit the factor $\exp(iKz)$ because it does not influence the intensity. The transmission amplitude is well known^[14,25,26] and can be written in the form convenient for calculations

$$A_0(q, t) = \frac{\exp(M + G) + x_1^2 \exp(M - G)}{1 + x_1^2} \quad (6)$$

Here

$$M = i[X_0 + \alpha_q] \frac{t}{2\gamma_0}, \quad G = ig \frac{t}{2\gamma_0}, \quad g = (\alpha_q^2 + X^2)^{1/2}, \quad (7)$$

$$x_1 = \frac{\alpha_q + g}{X}, \quad X_0 = K\chi_0, \quad X = K(\chi_h \chi_{-h})^{1/2},$$

$$\alpha_q = (q - q_0) \sin(2\theta_B), \quad \gamma_0 = \cos(\theta_B)$$

The parameter g has a positive imaginary part; χ_0 , χ_h , and χ_{-h} are the Fourier components of crystal susceptibility for the reciprocal lattice vectors $\mathbf{0}$, \mathbf{h} , and $-\mathbf{h}$; θ_B is the Bragg angle; the parameter $q_0 = K\theta_0$ describes a possible deviation of the crystal orientation from the Bragg position.

The similar equation can be written for the reflected wave with the base wave vector $\mathbf{k}_0 + \mathbf{h}$

$$E_h(x, t_1) = (\lambda L)^{1/2} \int \frac{dq}{2\pi} \exp(iqx) P_r(q, L) A_h(q, t_1) \quad (8)$$

where

$$A_h(q, t) = \frac{X_h}{2g} [\exp(M + G) - \exp(M - G)] \quad (9)$$

Here $X_h = K\chi_h$.

At the second step, we consider diffraction of the X-ray monochromatic inhomogeneous wave inside the crystal slab having an inhomogeneous structure along the crystal surface. At this point, the x and z coordinates are counted along and normal to the crystal surface. This task has to be solved by means of the Takagi equations^[3]

$$\frac{2}{i} \frac{\partial E_0}{\partial s_0} = X_0 E_0 + X_{-h} \exp(i\mathbf{h}\mathbf{u}) E_h \quad (10)$$

$$\frac{2}{i} \frac{\partial E_h}{\partial s_h} = [X_0 + 2\alpha_q] E_h + X_h \exp(-i\mathbf{h}\mathbf{u}) E_0 \quad (11)$$

Here $X_{-h} = K\chi_{-h}$, s_0 and s_h are the coordinates along the transmitted and reflected beams, \mathbf{u} is the displacement vector of possible deformation of the crystal lattice, $\alpha_q = K[\theta - \theta_0] \sin(2\theta_B)$ where θ and θ_0 are the deviations of the incident wave direction and crystal orientation from the Bragg position.

It is convenient to make the substitution $E_h = E'_h \exp(-i\mathbf{h}\mathbf{u})$ and write the equations in the other form

$$\frac{p}{2} \frac{\partial E_0}{\partial s_0} = A_0 E_0 + A E'_h, \quad \frac{q}{2} \frac{\partial E'_h}{\partial s_h} = B E_0 + [B_0 + W] E'_h \quad (12)$$

where

$$A_0 = iX_0 p/4, \quad A = iX_{-h} p/4, \quad B_0 = iX_0 q/4, \\ B = iX_h q/4, \quad W = i \left[\alpha_q + \frac{d\mathbf{h}\mathbf{u}}{ds_h} \right] \frac{q}{2} \quad (13)$$

In this work, we are interested in the task where \mathbf{u} is equal to zero (the perfect crystal), but the parameters χ_0 , χ_h , and χ_{-h} are not constant, i. e., they depend on the coordinates inside the crystal. Here p and q are the parameters which are determined during an approximate numerical solution of the Takagi equation. Namely, we consider a crystal slab with the surface parallel to the x axis. We divide it into the layers of the thickness d_z . Then p and q are the distances inside the layer along the transmitted and reflected beams. In the case of symmetrical Laue diffraction, $p = q = d_z/\gamma_0$.

We need to replace derivatives by difference ratios for numerical solution of Equation (12). We will use the method which was proposed by Epelboin,^[11] where the derivatives are calculated as

$$p \frac{df(x - p/2)}{dx} = f(x) - f(x - p) \quad (14)$$

In addition, the function values between the layer boundaries are calculated approximately as

$$2f(x - p/2) = f(x) + f(x - p) \quad (15)$$

We apply Equation (14) and (15) for Equation (12) and obtain a set of linear equations for the amplitudes of the transmitted and reflected waves at a set of points with the period d_z along the z axis and the period $d_x = 2d_z \tan \theta_B$ along the x axis.

The solution of these equations $E_2^{(\text{new})}$ can be calculated as a product of the Matrix $M_{2,4}$ and the vector $E_4^{(\text{old})}$, namely,

$$E_2^{(\text{new})} = M_{2,4} \times E_4^{(\text{old})} \quad (16)$$

where

$$E_2^{(\text{new})} = [E_0(s_0, s_h), E'_h(s_0, s_h)] \quad (17)$$

$$E_4^{(\text{old})} = [E_0(s_0^-, s_h), E'_h(s_0^-, s_h), E_0(s_0, s_h^-), E'_h(s_0, s_h^-)] \quad (18)$$

$$M_{2,4} = D^{-1} \begin{pmatrix} A_0^{(+)} W_1^{(-)}, A W_1^{(-)}, AB, A W_1^{(+)} \\ A_0^{(+)} B, AB, A_0^{(-)} B, A_0^{(-)} W_1^{(+)} \end{pmatrix} \quad (19)$$

Here $s_0^- = s_0 - p$, $s_h^- = s_h - q$,

$$A_0^{(\pm)} = 1 \pm A_0, \quad W_1^{(\pm)} = 1 \pm W_1, \\ W_1 = W + B_0, \quad D = A_0^{(-)} W_1^{(-)} - AB \quad (20)$$

We start with the entrance boundary of the first layer where the amplitudes E_0 and E'_h are known from the boundary conditions and apply the product $E_2^{(\text{new})} = M_{2,4} \times E_4^{(\text{old})}$ to obtain the values at the exit boundary which is the entrance boundary for the next layer. Thus, we obtain the amplitudes at all points along the x and z axes.

Note that the number of points along the x axis decreases by one in each step. Therefore, to obtain the solution inside the region of size $N_x d_x$ along the x axis, we need to know the boundary conditions inside a region of the size $(N_x + N_z) d_x$, and the thickness of the second part of the sample will be $t_0 = N_z d_z$ (see **Figure 2**). Here N_x is the number of periods on the exit surface of the crystal, and N_z is the number of layers.

If the crystal contains amorphous subareas inside the considered area, the matrix $M_{2,4}$ in such subareas has the form

$$M_{2,4} = D^{-1} \begin{pmatrix} A_1^{(+)} B_1^{(-)}, 0, 0, 0 \\ 0, 0, 0, A_1^{(-)} B_1^{(+)} \end{pmatrix} \quad (21)$$

where

$$A_1^{(\pm)} = 1 \pm A_1, \quad B_1^{(\pm)} = 1 \pm B_1, \\ A_1 = iX_1 p/4, \quad B_1 = iX_1 q/4, \quad D = A_1^{(-)} B_1^{(-)} \quad (22)$$

and $X_1 = K\chi_1$, χ_1 is the susceptibility of the amorphous area which can have another chemical composition. Inside the empty space $\chi_1 = 0$, and the matrix $M_{2,4}$ has a very simple form. In the symmetrical case $B_1 = A_1$.

In such an approach, the results of the first step form the boundary conditions for the second step. However, the sets of points in the first and second steps are different. Therefore, we need to interpolate the first set of points to the second one. In addition, it is necessary to consider the Bragg angle between the x axes at the first and second steps.

All equations were written for sigma polarization when the electric field vectors of the transmitted and reflected waves are directed normal to the scattering plane. Such a situation is typical for the experiments with synchrotron radiation. In the case of pi polarization, the parameters χ_h and χ_{-h} have to be multiplied by the factor $\cos(2\theta_B)$.

For a computer experiment, we have chosen a Si crystal, the photon energy $E = 8.048$ keV (CuK α characteristic radiation),

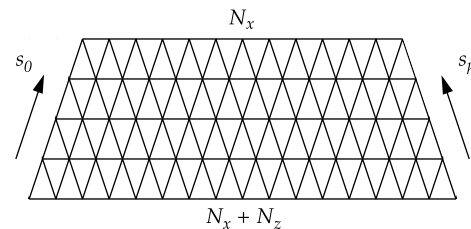


Figure 2. Set of points for a numerical solution of the Takagi equations.

and the 220 reflection. In this case, $\theta_B = 23.651^\circ$. The parameters χ_0 , χ_h , and χ_{-h} were calculated by means of the online computer program created by Kohn.^[27] Amplitudes in Equation (6) and (9) were normalized to the unit sum of the transmitted and reflected intensities at the Bragg angle when $\alpha_q = 0$.

Such normalization is useful for the large distance L when the incident spherical wave close to a plane wave near the triangular cutout. It is not the case for a small distance when the intensity at the detector becomes very small for a thick crystal. The reason for this is that a thick crystal selects only a small part of the angular width of the incident wave near the Bragg angle where the Borrmann effect takes place.

Fourier integrals in Equation (5) and (8) were calculated by means of the FFT (Fast Fourier Transform) procedure which was incorporated in the ACL programming language^[28]. Fortran code of this procedure has been known since the middle of the last century as a part of the NAG library. We use a set of points with the number $N = 16\,384$. We choose the step d_x , whereas $d_q = Kd_\theta = 2\pi/(Nd_x)$ and the calculation region in the reciprocal space Nd_q should be large enough the integrand to be zero out of this region.

Note that amplitude in Equation (6) equals $\exp(iX_0t/2\gamma_0)$ in the limit $|q| \rightarrow \infty$, and it is not zero for a thin crystal layer. That is why it is useful to consider finite angular divergence of the incident wave, i.e., the finite parameter α_d in Equation (1) and (2). In real experiments the angular divergence is always finite.

It is important to control a position of the Borrmann fan in space. Fourier integrals in Equation (5) and (8) give nonzero values only for $x < 0$, because the point $x = 0$ corresponds to all rays out of the Bragg diffraction region. It is convenient to shift the origin of the x axis so that the point $x = 0$ corresponds to the middle point of the Borrmann fan for the small distance L . Additional shift on the distance $x_s = -L\theta_0$ should be performed to correct the Bragg direction on the crystal.

A proper choice of the beam center is very important for a thick crystal layer because only the center of the Borrmann fan corresponds to rays in the center of dispersion surface of two-beam diffraction for which the anomalous transmission effect takes place. Such a shift may be performed by means of multiplying the integrand by the factor $\exp(iq[L\theta_0 - t \sin \theta_B])$.

The computer program was written in the ACL programming language.^[28] This language is interpreted by the program written in Java. It allows a user to quickly create the graphics and animations of numerical results.

3. Strong Intensity Increase Near the Triangular Cutout in a Thick Crystal

If the distance L is very large, for example, 25 000 m, the incident spherical wave is close to the plane wave. We consider the crystal layer of $t_1 = 800 \mu\text{m}$ before the cutout and a height of the cutout $t_0 = 150 \mu\text{m}$. The solution of the Takagi equations were obtained on a set of points with $d_z = 0.05 \mu\text{m}$, $N_z = 3000$, and $N_x = 3000$. The angle of the cutout was $\theta = 14.723^\circ$. In this case, $\tan(\theta)/\tan(\theta_B) = 0.6$.

The computer simulation results are shown in **Figure 3**. Note that normal absorption in the first layer is very large ($\mu_0 t_1 / \gamma_0 = 12.3$), whereas the anomalous absorption is acceptable

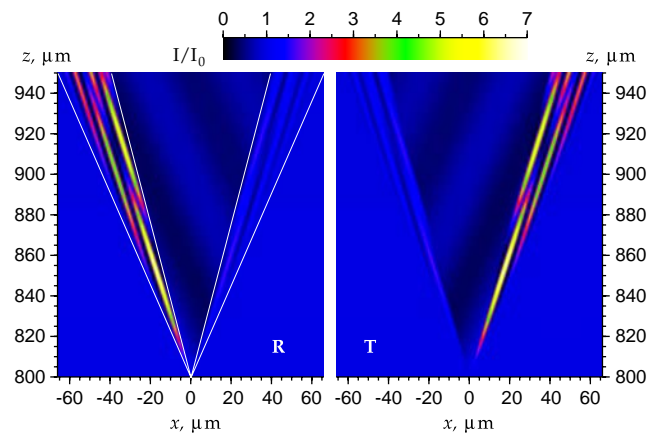


Figure 3. Intensity distribution in the area of an empty triangular cutout on the exit crystal surface.

($\mu_a t_1 / \gamma_0 = 0.38$). Here, $\mu_0 = \text{Im}(X_0)$, $\mu_a = \text{Im}(X_0 - X_h)$. Therefore, only the weakly absorbing wave reaches the cutout, and the extinction effect is absent. The intensity is homogeneous along the x axis because the incident wave is very close to a plane wave, and it depends very weakly on the z coordinate because the interference is absent.

The cutout disturbs the wave inside the Borrmann fan with the angle $2\theta_B$ (i.e., inside the triangle ade in **Figure 4**). We can distinguish three areas: A) the area of cutout (triangle bce); B) the left boundary region along the reflected beam (R-beam) direction (triangle abe); C) the right boundary region along the transmitted beam (T-beam) direction (triangle cde). The pictures for the R-beam and T-beam is shown in the **Figure 3** as R-picture and T-picture. They are fully antisymmetric.

Inside the region (A), we find the interference fringes with a small amplitude and a long period in the direction of the T-beam in the R-picture, and the R-beam in the T-picture. The most interesting is the effect of a strong intensity increase in the region (B) in the R-picture and in the region (C) in the T-picture. The maximum intensity in these regions is up to seven times higher compared with the intensity in the normal region.

To understand what happens, we need to get more information. Let us consider another case where the cutout is filled with a very strongly absorbing material that prevents passage of radiation through the cutout from one side region to another. The results of calculation in such a case are shown in **Figure 5**. We use the same intensity scale for the sake of comparison with **Figure 3**.

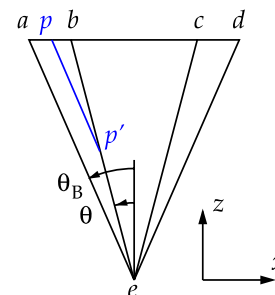


Figure 4. Borrmann fan with a triangular cutout. See text for details.

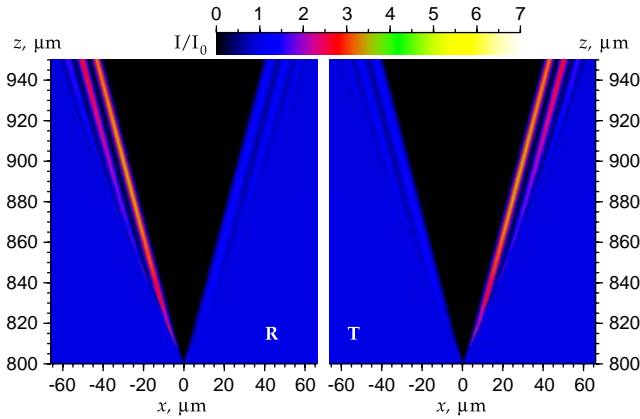


Figure 5. Intensity distribution in the area of a triangular cutout on the exit crystal surface filled by a strongly absorbing material.

In this case, the maximum intensity is two times smaller than that in Figure 3. In addition, the interference fringes are parallel to the boundary of the cutout. Inside the cutout, the intensity is zero due to strong absorption. It looks like in this case the interference of two rays takes place and the maximum intensity is slightly less than 4. In the case of Figure 3, the interference is three rays occurs and the maximum intensity is slightly less than 9. The third ray goes from one side to the other one through the empty space.

The results of Figure 3 were obtained previously in the work^[23] in the case of an incident plane wave by means of applying the crystal propagator. In that work, the corrections to the wave amplitude in an undisturbed crystal were considered, namely,

$$e_k(\mathbf{r}) = (E_k(\mathbf{r}) - A_k(z))F_0^{-1}(z), \quad k = 0, h, \quad (23)$$

where $E_k(\mathbf{r})$ are the solutions of Takagi Equation (10) and (11), $A_k(z)$ are the solutions for the undisturbed crystal. If $\alpha_q = 0$, in the case of a thick crystal, the approximation

$$A_k(z) = C_k F_0(z) F_h^{-1}(z), \quad F_{0,h}(z) = \exp(iX_{0,h}z/2\gamma_0) \quad (24)$$

is valid, as it follows from Equation (6) and (9). Here C_k is the constant.

Let us consider the region (B) in the R-picture. We are interested in $e_h(\eta)$ on the line $z = t$ where $\eta = x_0 - x$, x_0 is the coordinate at the cutout boundary (the point b in Figure 4). We can write the integral equation^[23] as follows

$$e_h(\eta) = e_h(\xi_\eta) - \frac{1}{4}b^2\varepsilon\eta \int_0^{\xi_\eta} d\xi e_h(\xi) \times U(b[(\xi_\eta - \xi)(\xi_\eta - \xi + \varepsilon\eta)]^{1/2}) \quad (25)$$

where

$$U(x) = 2\frac{J_1(x)}{x}, \quad \xi_\eta = \xi_0 - \eta D, \quad \xi_0 = \frac{t_0}{\gamma}, \quad (26)$$

$$D = \frac{\gamma_0}{\sin(\theta_B - \theta)}, \quad \varepsilon = D + \frac{\gamma_0}{\sin(\theta_B + \theta)}, \quad \gamma = \cos(\theta)$$

Here, $J_1(x)$ is the Bessel function of the first order; the integral is calculated along the left boundary of the triangular cutout from t_1 to $z_\xi = t_1 + \gamma\xi$

$$b = X \frac{[\sin(\theta_B - \theta) \sin(\theta_B + \theta)]^{1/2}}{\sin(2\theta_B)} \quad (27)$$

Derivation of Equation (25) is done in Appendix.

In the general case, the function $e_h(\xi)$ is not known. However, it is not the case if we consider a strong absorber as in Figure 5. In this case, $E_h(\xi) = 0$ and

$$e_h(\xi) = -A_h(z_\xi)F_0^{-1}(z_\xi) = -C_h F_h^{-1}(z_\xi) \quad (28)$$

Let us consider the ratio $R_h(\eta) = E_h(\eta)/A_h(t)$. Considering Equation (25) and (28), we obtain

$$R_h(\eta) = 1 - F_h(\gamma D\eta) + \frac{1}{4}b^2\varepsilon\eta \int_0^{\xi_\eta} d\xi F_h(t_0 - \gamma\xi) \times U(b[(\xi_\eta - \xi)(\xi_\eta - \xi + \varepsilon\eta)]^{1/2}) \quad (29)$$

We change an integration variable by the relation $\xi = \xi_\eta - \xi_1$ without a change in the limits and obtain finally

$$R_h(\eta) = 1 - F_h(\gamma D\eta)G(\eta) \quad (30)$$

where

$$G(\eta) = 1 - \frac{1}{4}b^2\varepsilon\eta \int_0^{\xi_\eta} d\xi_1 F_h(\gamma\xi_1)U(b[\xi_1(\xi_1 + \varepsilon\eta)]^{1/2}) \quad (31)$$

A peculiarity of Equation (30) is that it contains two terms, the second of which is complex valued. Therefore, the square modulus may demonstrate interference fringes with the constant period. We also note that the dependence on t_0 is defined by only the upper limit of integral in Equation (31). It is easy to understand that this dependence will be apparent only for small values of t_0 and only for η values close to $\eta_m = t_0/(\gamma D)$.

Figure 6 shows the curve $|R_h(\eta)|^2$ calculated by means of Equation (30) and (31) for $z = 950 \mu\text{m}$ and the parameters of Figure 5. One can see a good correspondence with the results of Figure 5 obtained by a direct solution of the Takagi equations. Note that the curve was improved for η close to η_m because Equation (28) is valid for all ξ except the region of very small values where a thickness of the absorbing material is small. We do not know $e_h(\xi)$ in this region, but we know that $e_h(0) = 0$.

Let us discuss physical basis of the effect of strong interference. In the region (B), the intensity of the R-beam has to be equal to zero at the cutout boundary because there is no incident wave in this boundary. As the radiation is not zero inside the

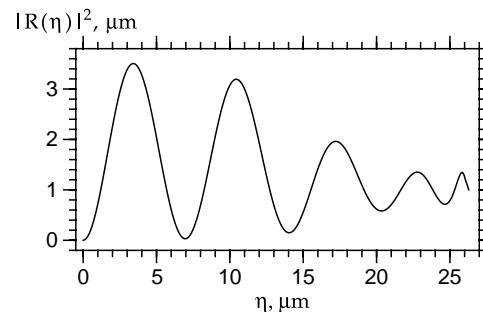


Figure 6. Intensity distribution in a part of the area of a triangular cutout on the exit crystal surface filled with a strongly absorbing material.

crystal, the most simple method to make zero intensity is to create a standing wave due to interference of two rays. In contrast, the intensity of the R-beam has to be close to a constant at the Borrmann fan boundary. Therefore, the amplitude of the standing wave has to decrease strongly on the way from the first boundary to the second one. We can see such a behavior of the intensity in Figure 6.

4. Distance Dependence of the Effect of a Strong Intensity Increase

There are many parameters of the task considered in this work. The first one is the distance L between the point source and the crystal. The second one is the thickness t_1 of the perfect crystal layer. The third one is the crystal angular deviation θ_0 from the Bragg position. The fourth one is the angle θ of the triangular cutout. The fifth one is the shift Δx of the crystal relative to the incident beam when the triangular cutout position may be slightly out of the beam center. In this work, we discuss only the distance dependence.

The direct numerical calculations show that when L decreases from 25 000 to 50 m, the picture of Figure 3 remains approximately the same with one difference in the base intensity value I_0 . Figure 3 shows the relative intensity $I(x, z)/I_0$; the value I_0 is not shown. It is assumed that the value I_0 corresponds to the bottom line of the figure.

According to Equation (3), the spherical wave intensity is equal to unity on the entrance surface of the crystal. If the incident wave is close to the plane wave, the intensity of the transmitted and diffracted waves for the crystal of the thickness $t_1 = 800 \mu\text{m}$ is close to $0.25 \exp(-0.38) = 0.171$ due to the Borrmann effect. However, there is a diffraction focusing effect^[12,13,29] for the distance $L_0 = C_0 t$, where $C_0 = |\chi_h|^{-1} \sin(\theta_B) \sin(2\theta_B)$. In our case, $C_0 = 3.17 \times 10^4$. For the thickness t_1 , we have $L_0 = 25.4 \text{ m}$.

For this distance, the beam width inside the crystal becomes less than the width of the Borrmann fan $W_0 = 2t_0 \tan(\theta_B)$ near the triangular cutout. In addition, the maximum beam intensity becomes 20 times higher. If the distance L is greater than 50 m, the intensity increases due to the focusing effect, but the beam width is rather large compared with W_0 . As a result, the calculated picture of normalized intensity remains approximately the same as in Figure 3.

It is interesting that approximately the same pictures, as in Figure 3, were calculated for the distance L less than 10 m. However, now the base intensity value I_0 is rather small and it decreases with a decrease in the distance. The reason for this is that in this case the beam becomes divergent with a rather large angular width. A thick crystal works as a collimator and it selects the narrow angular width near the Bragg angle where an anomalous transmission takes place. However, it is only a small part of total intensity. We can call this phenomenon as the antifocusing effect.

A very strong change in the picture occurs for distances near the focusing distance L_0 . Figure 7 shows color maps of intensity distribution for $L = 30 \text{ m}$ (top panel), 25 m (middle panel), and 20 m (bottom panel). In the top panel, the beam width decreases with an increase in the thickness; in the bottom panel, the beam width increases with an increase in the thickness; and in the

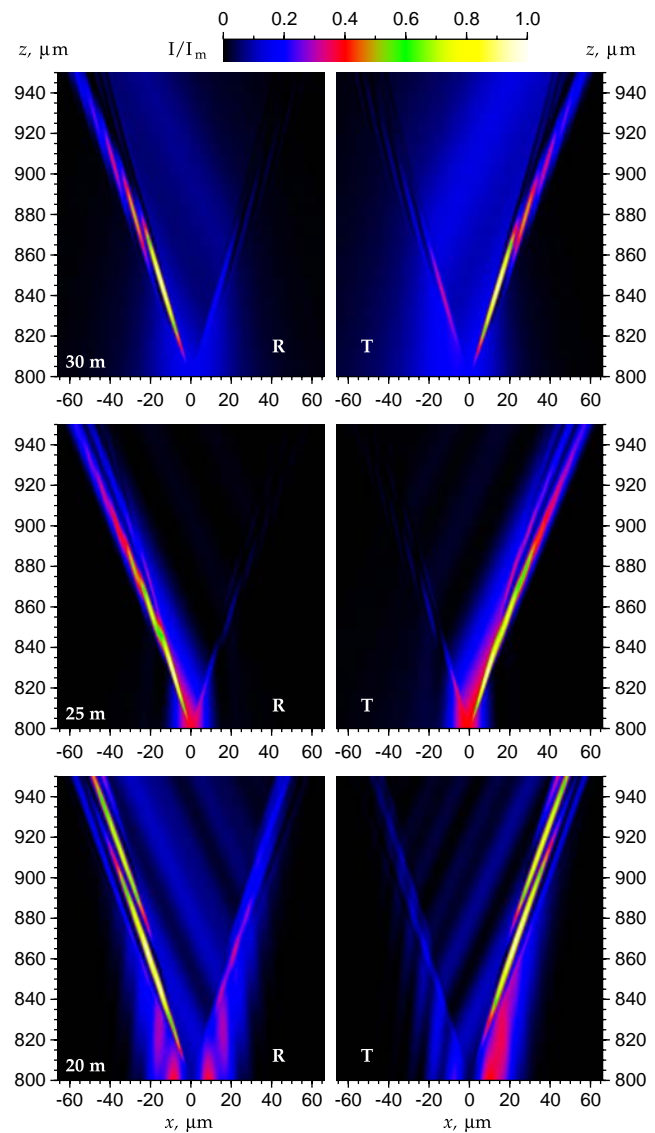


Figure 7. Intensity distribution in the area of an empty triangular cutout on the exit crystal surface for various distances $L = 30 \text{ m}$ (top panel), 25 m (middle panel) and 20 m (bottom panel).

middle panel, the focus position is just in front of the beginning of the cutout.

Despite the fact that the pictures have a rather complicated structure, the intensity increase effect takes place in all the cases. In this figure, the intensities on the maps are normalized to the maximum value. Let us denote the value of reflectivity on the bottom line of the pictures as R_1 and the maximum value as R_m and the same for transmissivity replacing R by T .

Then, if the plane wave reflectivity and transmissivity at the Bragg angle are normalized by 0.5 (the sum is equal to unity), we obtain the following values: $R_1 = 3.0$, $R_m = 18.3$, $T_1 = 3.8$, $T_m = 15.5$ for $L = 30 \text{ m}$, $R_1 = 7.8$, $R_m = 20.2$, $T_1 = 8.1$, $T_m = 20.3$ for $L = 25 \text{ m}$, and $R_1 = 3.7$, $R_m = 9.3$, $T_1 = 5.5$, $T_m = 13.3$ for $L = 20 \text{ m}$. Note that R_m and T_m have higher values if θ is close to θ_B and lower values with decreasing θ .

5. Conclusion

The standard theory of X-ray Laue diffraction in a perfect crystal considers a crystal such as a slab with an infinite lateral size. Two wave fields have been discovered inside the crystal for which strong and weak absorption takes place. As a result, the interference fringes can be observed in a thin crystal with a period of extinction length. In a thick crystal, only one field exists and the fringes are absent.

We have found out that if the crystal has a triangular cutout on the exit surface, new kind of fringes can be observed. In addition, the intensity maximum can increase up to seven times. In this case, the boundary conditions become rather complicated, and it is simpler to obtain the results by means of a direct numerical solution of the Takagi equations with the Fourier components of crystal susceptibility variable in space. We show that the calculations based on the crystal propagator lead to the same results but can give better understanding of the intensity increase effect.

Appendix: Derivation of Equation (25)

The integral equations for the wave amplitudes $E_k(\mathbf{r})$ were derived by Afanasev and Kohn^[8] from Takagi equations (10) and (11). The same equations are valid for the additional wave amplitude $e_k(\mathbf{r})$. In our case of a perfect single crystal, the wave field $e_h(\mathbf{r})$ on the line ab is defined by the wave fields $e_k(\mathbf{r})$ on the line aeb (see Figure 4). However, these fields are equal to zero on the line ae . Therefore

$$e_h(p) = e_h(p') - \int_{ep'} ds_0 \frac{\partial R}{\partial s_0} e_h - \frac{i}{2} X_h \int_{ep'} ds_h R e_0 \quad (32)$$

Here, the coordinates s_0, s_h are defined in Equation (10) and (11) and

$$R = J_0(X((s_{0p} - s_0)(s_{hp} - s_h))^{1/2}) \quad (33)$$

where $J_0(x)$ is the Bessel function of zero order. The field $e_0(p')$ on the line be is a solution of the integral equation

$$e_0(p') = \int_{ep'} ds_h \frac{\partial R}{\partial s_h} e_0 + \frac{i}{2} X_{-h} \int_{ep'} ds_0 R e_h \quad (34)$$

In our particular case of a triangular cutout, Equation (34) can be solved by means of the Laplace transform and we have the following results

$$e_0(\xi_\eta) = iX_{-h}\gamma_1 \int_0^{\xi_\eta} d\xi U(b[\xi_\eta - \xi])e_h(\xi) \quad (35)$$

where ξ_η is the coordinate of the point p' on the line be and

$$\gamma_1 = \frac{\sin(\theta_B - \theta)}{\sin(2\theta_B)} \quad (36)$$

We substitute Equation(35) into Equation (32) and apply the Laplace transform once again. As a result, we obtain Equation (25).

Conflict of Interest

The authors declare no conflict of interest.

Keywords

strong intensity increase, thick crystal, triangular cutout, X-ray diffraction, X-ray interference effect, X-ray topography

Received: July 22, 2019

Revised: September 8, 2019

Published online: October 4, 2019

-
- [1] N. Kato, A. Lang, *Acta Cryst.* **1959**, *12*, 787.
 [2] N. Kato, *Acta Cryst.* **1961**, *14*, 526.
 [3] S. Takagi, *Acta Cryst.* **1962**, *15*, 1311.
 [4] I. Sh Slobodetskii, F. N. Chukhovskii, V. L. Indenbom, *Pis'ma ZhETF* **1968**, *8*, 90.
 [5] T. S. Urugami, *J. Phys. Soc. Jpn.* **1969**, *27*, 147.
 [6] T. S. Urugami, *J. Phys. Soc. Jpn.* **1970**, *28*, 1508.
 [7] T. S. Urugami, *J. Phys. Soc. Jpn.* **1971**, *31*, 1141.
 [8] A. M. Afanas'ev, V. G. Kohn, *Acta Cryst.* **1971**, *27*, 421.
 [9] T. Saka, T. Katagawa, N. Kato, *Acta Cryst. A* **1971**, *28*, 102.
 [10] T. Saka, T. Katagawa, N. Kato, *Acta Cryst. A* **1971**, *28*, 113.
 [11] Y. Epelboin, *Acta Cryst.* **1977**, *33*, 758.
 [12] A. M. Afanas'ev, V. G. Kohn, *Fiz. Tverd. Tela* **1977**, *19*, 1775.
 [13] A. M. Afanas'ev, V. G. Kohn, *Sov. Phys. Solid State* **1977**, *19*, 1035.
 [14] A. Authier, *Dynamical Theory of X-ray Diffraction*, 3rd edition. Oxford University Press, Oxford, UK **2005**.
 [15] N. M. Olekhovich, A. I. Olekhovich, *Acta Cryst. A* **1978**, *34*, 321.
 [16] N. M. Olekhovich, A. I. Olekhovich, *Acta Cryst. A* **1980**, *36*, 22.
 [17] D. K. Saldin, *Acta Cryst. A* **1982**, *38*, 425.
 [18] T. S. Urugami, *J. Phys. Soc. Jpn.* **1983**, *52*, 3073.
 [19] E. V. Shulakov, I. A. Smirnova, E. V. Suvorov, *Poverkhnost'* **1996**, *7*, 32.
 [20] E. V. Shulakov, I. A. Smirnova, E. V. Suvorov, *Surface Investig.* **1997**, *12*, 799.
 [21] V. I. Punegov, S. I. Kolosov, K. M. Pavlov, *J. Appl. Cryst.* **2016**, *49*, 1190.
 [22] A. G. Shabalin, O. M. Yefanov, V. L. Nosik, V. A. Bushuev, I. A. Vartanyants, *Phys. Rev. B* **2017**, *96*, 064111.
 [23] A. M. Afanas'ev, V. G. Kohn, *Ukr. Fiz. Zh.* **1972**, *17*, 424.
 [24] V. G. Kohn, *J. Synchrotron Radiat.* **2018**, *25*, 1634.
 [25] Z. G. Pinsker, *Dynamical Scattering of X-Rays in Crystals*, Springer-Verlag, Berlin **1978**.
 [26] V. G. Kohn, *Phys. Status Solidi B* **2002**, *231*, 132.
 [27] Program, <http://kohnvict.ucoz.ru/jsp/3-difpar.htm> (accessed: 2018).
 [28] Website, <http://kohnvict.ucoz.ru/acl/acl.htm> (accessed: 2017).
 [29] V. G. Kohn, I. A. Smirnova, *Acta Cryst. A* **2018**, *74*, 699.